Hf-W Chronometry of Lunar Metals and the Age and Early Differentiation of the Moon

Thorsten Kleine,[1,2]* Herbert Palme,[3] Klaus Mezger,[1] Alex N. Halliday[2,4]

The use of hafnium-tungsten chronometry to date the Moon is hampered by cosmogenic tungsten-182 production mainly by neutron capture of tantalum-181 at the lunar surface. We report tungsten isotope data for lunar metals, which contain no [181]Ta-derived cosmogenic [182]W. The data reveal differences in indigenous [182]W/[184]W of lunar mantle reservoirs, indicating crystallization of the lunar magma ocean 4.527 ± 0.010 billion years ago. This age is consistent with the giant impact hypothesis and defines the completion of the major stage of Earth's accretion.

The most widely accepted model for the formation of the Moon involves a catastrophic collision between a Mars-sized body and the proto-Earth. This giant impact most likely occurred during the final stages of accretion and contributed roughly the last 10% of Earth's mass (1). As such, the age of the Moon provides the best time marker for the completion of Earth's accretion. Long-lived chronometers have been used to date ancient lunar rocks to 4.56×10^9 to 4.29×10^9 years ago (Ga) (2–4), but the Moon's exact age has been uncertain.

Hafnium-182 decays to [182]W with a half-life of 8.9×10^6 years (My) and is well suited to constrain the time of the Moon's formation (5–7). However, enhanced [182]W/[184]W in lunar samples (5) largely reflect cosmogenic [182]W added from neutron capture of [181]Ta during the intense cosmic ray exposure of the lunar surface (8, 9). The large corrections introduce uncertainties that exceed the anticipated [182]W/[184]W variations produced in the lunar interior, compromising a reliable interpretation in terms of [182]Hf-[182]W chronometry. Almost all lunar samples contain small amounts of metal, which is enriched in W and contains no detectable Ta (10) [Supporting Online Material (SOM) Text 1]. Hence, lunar metals should not carry a cosmogenic [181]Ta-derived component. Here, we analyzed these metals to date the formation of the Moon and the crystallization of the lunar magma ocean (LMO) thought to be formed by the giant impact.

Obtaining a Hf-W chronology requires significant variation in Hf/W among the rocks produced in the LMO. The first rocks to crystallize from the LMO consisted mainly of olivine and pyroxene. These were followed by plagioclase-rich cumulates (ferroan anorthosites) that floated to the surface, forming the earliest lunar crust (11). The end of the crystallization sequence involved the precipitation of ilmenite and clinopyroxene until solidification of the last few percents of the magma ocean (11, 12). The characteristic features of this residual liquid [termed KREEP for high contents of potassium (K), rare earth elements (REE), and phosphorus (P)] are its strong enrichment in incompatible elements and its uniform elemental and isotopic composition, resulting from global-scale lunar differentiation (12, 13). Subsequent melting and mixing among these primary rocks produced the variety observed in the lunar sample suite (11). For example, mare basalts formed by remelting of early mafic cumulates, which in the case of high-Ti mare basalts included assimilation of ilmenite-clinopyroxene. The redistribution of KREEP during impacts on the lunar surface resulted in the contamination of most highland breccias with KREEP, making KREEP the major carrier of incompatible elements in lunar highland rocks. Hf-W fractionations in the crystallizing LMO result from the high incompatibility of W and the compatibility of Hf in clinopyroxene-ilmenite, leading to low Hf/W in KREEP and complementary high Hf/W in the high-Ti mare basalt source (6, 7, 14). If these Hf-W fractionations occurred during the effective lifetime of [182]Hf, variations in the [182]W/[184]W of lunar mantle reservoirs will result.

[1]Zentrallabor für Geochronologie, Institut für Mineralogie, Corrensstrasse 24, D-48149 Münster, Germany. [2]Departement für Erdwissenschaften, Institut für Isotopengeologie und Mineralische Rohstoffe, Sonneggstrasse 5, Eidgenössische Technische Hochschule (ETH) Zentrum NO, CH-8092 Zürich, Switzerland. [3]Institut für Geologie und Mineralogie, Universität zu Köln, Zülpicherstrasse 49b, D-50674 Köln, Germany. [4]Department of Earth Sciences, Oxford University, Parks Road, Oxford OX1 3PR, UK.

*To whom correspondence should be addressed. E-mail: kleine@erdw.ethz.ch

Table 1. W isotope data and Ta/W and Hf/W for lunar metals and whole rocks. $\varepsilon_W = \{[(^{182}W/^{184}W)_{meas} - (^{182}W/^{184}W)_{std}]/(^{182}W/^{184}W)_{std}\} \times 10^{-4}$. W, Hf, and Ta concentration data are given in table S1. Techniques for the separation of metals and analytical methods for W isotope measurements are described elsewhere (28, 29). All measurements were performed with the IsoProbe (GV Instruments, Manchester, UK) multiconductor inductively coupled plasma mass spectrometer (MC-ICPMS) (28) at Universität Münster except those labeled with an asterisk. $\Delta\varepsilon_{W,GCR}$ is the shift in ε_W caused by the interaction with galactic cosmic rays (GCR) and is calculated only for metals by using corrections equations (15) and published exposure ages (reference listed in table S2). Details about these correction calculations are given in SOM Text. Corrected ε_W values are obtained as $\varepsilon_{W,corr} = \varepsilon_{W,meas} - \Delta\varepsilon_{W,GCR}$. Repl., replicate.

Sample	Exposure age (Ma)	$\varepsilon_{W,meas} \pm 2\sigma$	$\Delta\varepsilon_{W,GCR} \pm 2\sigma$	$\varepsilon_{W,corr} \pm 2\sigma$
		KREEP-rich samples		
14310 metal	300	−0.10 ± 0.50	−0.26 ± 0.13	0.16 ± 0.52
15445 metal	220	−0.54 ± 0.50		
Repl.	"	0.24 ± 0.50		
Repl.*	"	0.09 ± 0.50		
Mean	"	−0.07 ± 0.29	−0.19 ± 0.10	0.12 ± 0.30
62235 metal	163	−0.39 ± 0.50		
Repl.*	"	0.00 ± 0.50		
Repl.*	"	−0.12 ± 0.50		
Mean	"	−0.17 ± 0.29	−0.14 ± 0.07	−0.03 ± 0.30
62235 whole rock	"	0.80 ± 0.50		
65015 metal	490	−0.54 ± 0.50		
Repl.	"	−0.99 ± 0.50		
Repl.*	"	−1.01 ± 0.50		
Mean	"	−0.85 ± 0.29	−0.43 ± 0.22	−0.42 ± 0.36
65015 whole rock	"	2.40 ± 0.50		
78155 metal	30	−0.39 ± 0.80		
		Low-Ti mare basalts		
15475 metal	529	0.70 ± 0.96	−0.46 ± 0.23	1.16 ± 0.99
15475 whole rock	"	1.00 ± 0.50		
15555 whole rock	80	0.50 ± 0.80		
		High-Ti mare basalts		
72155 metal		1.74 ± 0.72		
72155 whole rock		1.40 ± 1.20		
79155 metal	575	2.31 ± 0.90	−0.51 ± 0.26	2.82 ± 0.94
79155 whole rock	"	37.90 ± 0.80		

*Measurement performed with the Nu Plasma (Nu Instruments, Wrexham, UK) MC-ICPMS at ETH Zürich (9).

We measured the W isotopic composition of eight lunar metals and six whole-rock samples (Table 1). The lunar metals have ε_W values (ε_W defined in Table 1) below or similar to the values obtained for their host rocks (Table 1 and Fig. 1). These differences are most pronounced for samples having old exposure ages and high Ta/W (samples 79155 and 65015) and are lower for samples with lower Ta/W and/or younger exposure ages (Fig. 1B and Table 1). These results corroborate suggestions that enhanced $^{182}W/^{184}W$ in lunar whole-rock samples largely reflect cosmogenic ^{182}W additions via neutron capture of ^{181}Ta (8, 9).

The $^{182}W/^{184}W$ of lunar metals could have been slightly lowered by neutron capture of W isotopes during cosmic ray exposure at the lunar surface. In contrast to the substantial ^{182}W production by neutron capture of ^{181}Ta, the effects of ^{182}W burnout are small (8, 15) and require only corrections that in most cases are smaller than the uncertainty of the W isotope measurements. Exposure ages for the KREEP-rich samples we examined range from ~160 to ~500 My, but the metals of these samples have similar ε_W values, providing further evidence that the effects of ^{182}W burnout are small. Sample 65015 has the longest exposure time and appears to have a slightly, albeit barely resolvable, lower ε_W compared to the other KREEP metals. This difference disappears after the effects of ^{182}W burnout are taken into account (Table 1, Fig. 2, and SOM Text 2). The lower exposure ages for samples 14310, 15445, and 62235 require corrections that are smaller than the analytical uncertainty of the W isotope measurements, indicating that the W isotope composition of KREEP can reliably be deduced from these samples, yielding an average ε_W of 0.06 ± 0.20 (2σ).

Low-Ti mare basalt 15555 shows no resolvable cosmogenic ^{182}W effects (9), and its average ε_W is 1.18 ± 0.20 [this study and (9)], identical to the corrected value for the metal of sample 15475 (Fig. 2). The exposure time of high-Ti mare basalt 72155 is unknown, but the similarity in the metal and whole-rock data in conjunction with a high Ta/W of ~20 in the bulk sample suggest only minor cosmic ray–induced shifts in the metal and bulk rock. This is consistent with the fact that the measured ε_W of the 72155 metal is indistinguishable from the corrected ε_W of the 79155 metal. High-Ti mare basalts thus have an indigenous W isotope composition (weighted mean $\varepsilon_W = 2.14 \pm 0.57$) that is slightly more radiogenic than that of low-Ti mare basalts ($\varepsilon_W = 1.18 \pm 0.20$) and significantly more radiogenic than that of KREEP ($\varepsilon_W = 0.06 \pm 0.20$) (Fig. 2).

The $^{182}W/^{184}W$ variations require the existence of at least three major lunar mantle reservoirs that acquired their distinct Hf/W ratios during the effective lifetime of ^{182}Hf. Determination of Hf-W ages requires knowledge of the Hf/W ratios in the source areas

prevailing during ^{182}Hf decay. Measured Hf/W ratios of lunar samples are the complex product of multiple melting events and do not provide a firm measure of the Hf/W ratio in the sources. Age information can be obtained by assuming the maximum range of Hf/W that can have been generated in the source areas. The uncertainties inherent in these estimates have little effect on the robustness of the calculated ages, because these are largely constrained by the well-resolved ε_W differences.

The range in ε_W values that could have been produced in the lunar mantle is illustrated in Fig. 3A. The $^{182}W/^{184}W$ variations are expressed as the deviation from the bulk LMO as represented by the $^{182}W/^{184}W$ ratio of low-Ti mare basalts. Their source region consists of olivine and orthopyroxene cumulates, the crystallization of which did not involve any substantial Hf-W fractionation (14). This is consistent with the absence of ^{142}Nd anomalies (from the decay of ^{146}Sm) in these rocks (16).

Palme and Rammensee (17) estimated U/W = 1.93 for the lunar mantle, corresponding to Hf/W = 26.5. This Hf/W ratio is similar to measured values for low-Ti mare basalts (table S1) (5), consistent with limited Hf-W fractionation during melting of olivine-orthopyroxene cumulates (14).

The relatively low ε_W of KREEP requires that its source evolved with a Hf/W ratio below that of the low-Ti mare basalt source, consistent with Hf/W ~ 12 to 19 for the KREEP source (12, 13). Measured Hf/W ratios of ~20 for KREEP-rich samples provide an upper limit to the Hf/W ratio because KREEP constitutes the reservoir with the lowest Hf/W ratio in the lunar mantle; contamination of KREEP with other mantle sources can only have increased the Hf/W ratio. The redistribution of KREEP during impacts on the lunar surface involved no Hf-W fractionation, as indicated by the uniform chemical composition of KREEP. Given the higher in-
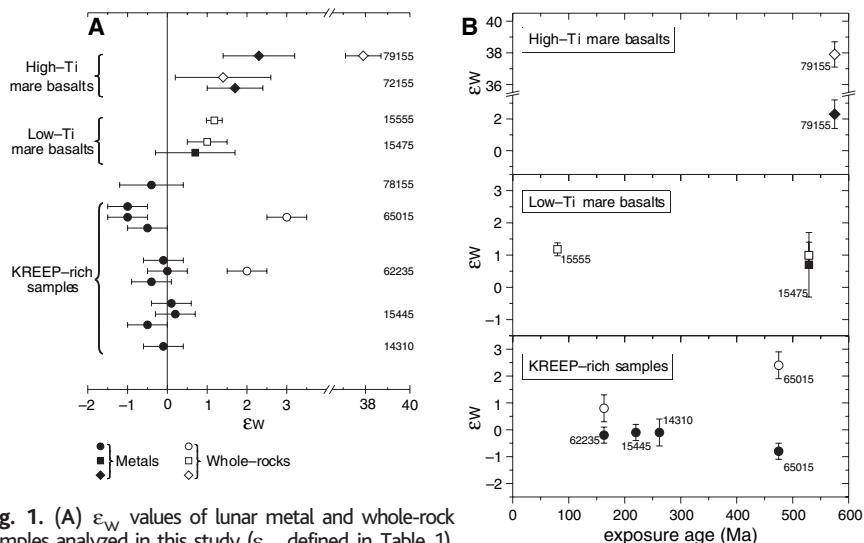

Fig. 1. (A) ε_W values of lunar metal and whole-rock samples analyzed in this study (ε_W defined in Table 1). The data point for 15555 is a weighted average calculated from the combined data from this study and Lee *et al.* (9). **(B)** ε_W versus exposure age for lunar metals and whole-rock samples. Exposure ages are from the literature (table S2). The ε_W values for whole-rock samples depend on both Ta/W (Table 1) and exposure age. In contrast, metals contain no Ta and hence no cosmogenic ^{182}W. Error bars indicate 2σ.
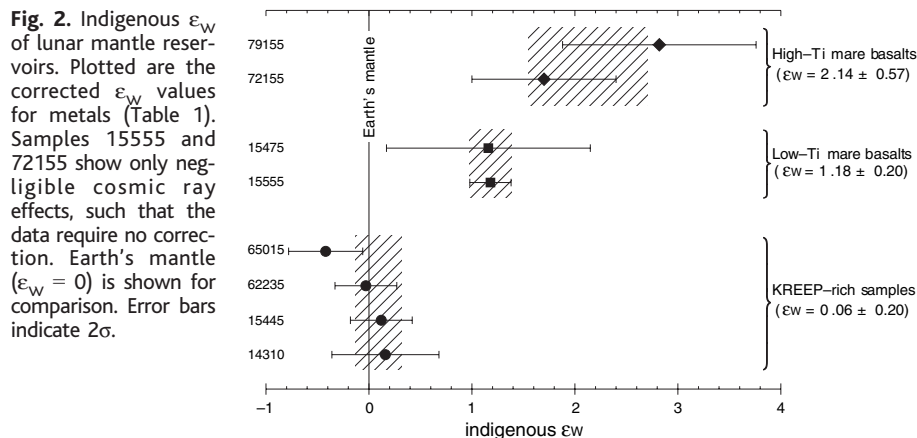

Fig. 2. Indigenous ε_W of lunar mantle reservoirs. Plotted are the corrected ε_W values for metals (Table 1). Samples 15555 and 72155 show only negligible cosmic ray effects, such that the data require no correction. Earth's mantle ($\varepsilon_W = 0$) is shown for comparison. Error bars indicate 2σ.

compatibility of W relative to Hf, partial melting in the high-Ti mare basalt source should result in a lower Hf/W ratio in the melt compared with the residue, implying that the source Hf/W ratio should be higher than that measured for high-Ti mare basalts (up to ~110). These basalts, however, formed several hundreds of millions of years after the primary differentiation of the Moon, such that their Hf/W ratio will reflect the increasing degree of source depletion by multiple melt extractions. On the basis of Hf and W partition coefficients, Righter and Shearer (14) calculated Hf/W > 40 for the high-Ti mare basalt source, implying a lower Hf/W ratio in the original reservoir than in high-Ti mare basalts themselves, consistent with their only slightly enhanced $^{182}W/^{184}W$ ratio.

Regardless of any uncertainties inherent in the estimated source Hf/W ratio, the latest possible time of differentiation can be obtained by assuming Hf/W = 0 for the reservoir with the lowest ε_W (i.e., the KREEP source). This age constraint is independent of any uncertainties in the Hf/W ratio of the KREEP source. If Hf/W = 0, the $^{182}W/^{184}W$ difference between KREEP and low-Ti mare basalts must have been generated no later than ~50 My after formation of calcium-aluminum-rich inclusions (CAIs) (Fig. 3). This is the latest possible time for differentiation because KREEP likely has Hf/W > 0, in which case less time is required to generate the ε_W difference between the KREEP and low-Ti mare basalt sources (Fig. 3). This age constraint is not very sensitive to uncertainties in the estimated Hf/W ratio of the bulk LMO, because a 50% variation in the Hf/W ratio of the bulk LMO (i.e., from 20 to 33) would result in an uncertainty of only ±3 My in the above age estimate. The latest possible time for dif-

ferentiation in the high-Ti mare basalt source is less well constrained (mainly reflecting uncertainties in the upper limit of the source Hf/W) but is consistent with the ~50-My age estimate derived for KREEP (Fig. 3).

The earliest possible time of lunar differentiation is less well constrained because it must rely on independent estimates of Hf/W ratios in the different reservoirs. However, both the upper limit of Hf/W < 20 in the KREEP source and the lower limit of Hf/W > 40 in the high-Ti mare basalt source constrain the earliest possible time of differentiation to ~30 My (Fig. 3). This is consistent with ~30-My W model ages for the Moon (18–20), which some authors (21, 22) interpret as the earliest possible time the Moon could have formed. This suggests that the upper and lower limits for the KREEP and high-Ti mare basalt sources, respectively, are reasonable.
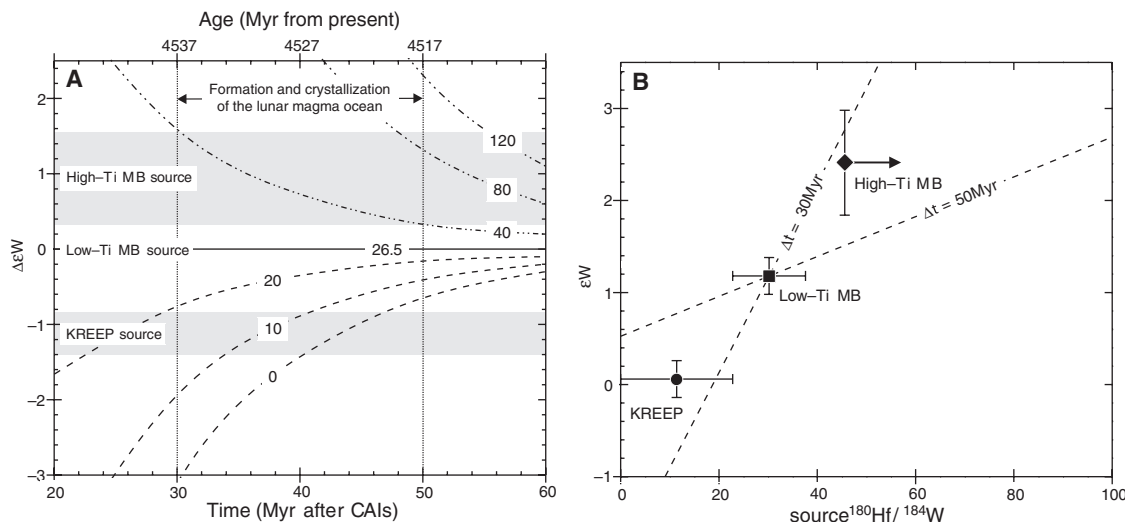
The preservation of W isotopic variations indicates that there was negligible mixing in the lunar interior since its earliest differentiation, because any W isotopic variability would have been effectively erased by convective overturn in a largely molten magma ocean. Thus, the LMO must have formed and crystallized from 30 to 50 My after the start of the solar system, i.e., 4.537 to 4.517 Ga. Three observations suggest that the observed ε_W variations directly result from Hf-W fractionation in the final stages of LMO crystallization. First, the W isotopic variations correlate with Hf/W ratios anticipated for fractionation in a crystallizing LMO (Fig. 3B). Second, KREEP is strongly enriched in W, such that resetting the W isotopic composition of KREEP would require substantial isotopic exchange between KREEP and the other reservoirs of the lunar mantle. It is thus more likely that KREEP preserved the W isotope

composition acquired at the final stage of LMO crystallization. Third, mixing of late-stage ilmenite-clinopyroxene cumulates with olivine as a result of cumulate overturn (23) would only shift the data point for the high-Ti mare basalt source downward to lower Hf/W ratios and ε_W values along the reference isochron (Fig. 3B). However, even if the $^{182}W/^{184}W$ variations did reflect post-LMO events, the Hf-W age would still provide the latest possible time for the crystallization of the LMO.

Rapid crystallization of the LMO 30 to 50 My after solar system formation contrasts with models that involve a long-lived (100 to 200 My) magma ocean (24), implying that the earliest lunar crust was not insulating enough to prevent rapid heat loss (7, 14). The ferroan anorthosites are regarded as remnants of the earliest lunar crust and if so must have formed before complete solidification of the magma ocean more than before 4.517 Ga. ^{147}Sm-^{143}Nd ages for some ferroan anorthosites [e.g., 4.44 ± 0.02 Ga for 60025 (2) and 4.29 ± 0.06 Ga for 62236 (4)], however, are younger, indicating that they do not date primary crust formation. Likewise, the ^{146}Sm-^{142}Nd model age of the lunar mantle [~4.32 Ga (16)] as well as Rb-Sr [4.42 ± 0.07 Ga (25)] and ^{147}Sm-^{143}Nd [4.36 ± 0.06 Ga (26)] model ages for KREEP are younger than the Hf-W age of >4.517 Ga. These younger ages must reflect post-LMO events such as remelting, mixing, and impact metamorphism. The latter might have aided to destabilize the earliest lunar crust, which is required for rapid cooling of the LMO (7).

The giant Moon-forming impact is the last major event in Earth's accretion (1), such that the date of this event should define the age of both the Earth and Moon. ^{182}Hf-^{182}W model ages for the Earth and Moon strongly depend

Fig. 3. (A) ε_W variations in the lunar mantle depending on Hf/W and time. Hf/W ratios between 0 and 120 cover the range of measured Hf/W ratios in lunar samples and estimated Hf/W ratios in the crystallizing LMO. $\Delta\varepsilon_W$ is the deviation of ε_W from the bulk LMO [ε_W = 1.18 ± 0.20, Hf/W = 26.5]. The numbers on curves indicate Hf/W ratios of the modeled reservoirs. The gray shaded areas indicate the ε_W deviation (expressed in $\Delta\varepsilon_W$) of the KREEP and high-Ti mare basalt sources from the low-Ti mare basalt source. Time of differentiation is calculated relative to $^{182}Hf/^{180}Hf$ = 1.07 × 10^{-4} ± 0.10 × 10^{-4} for CAIs (27). **(B)** ε_W versus $^{180}Hf/^{184}W$ in the sources. Reference isochrons corresponding to differentiation at 30 and 50 My after CAI formation are shown. Assumed Hf/W ratios are 10 ± 10 for KREEP, 26.5 ± 6.5 for the low-Ti mare basalt source, and >40 for the high-Ti mare basalt source. Error bars indicate 2σ.

on the model applied (particularly on the assumed degree of metal-silicate equilibration during core formation), resulting in age estimates ranging from ~30 to >100 My after solar system formation (20–22). In contrast, the Hf-W age of LMO crystallization tightly constrains the age of the Moon and the final stage of Earth's accretion to 30 to 50 My after the formation of the solar system. The formation of the Moon significantly later than that of asteroids and Mars (18, 27) underpins the Moon's origin by a unique event, as required in the giant impact hypothesis.

References and Notes

1. R. M. Canup, E. Asphaug, Nature 412, 708 (2001).
2. R. W. Carlson, G. W. Lugmair, Earth Planet. Sci. Lett. 90, 119 (1988).
3. C. Alibert, M. D. Norman, M. T. McCulloch, Geochim. Cosmochim. Acta 58, 2921 (1994).
4. L. E. Borg et al., Geochim. Cosmochim. Acta 63, 2679 (1999).
5. D.-C. Lee, A. N. Halliday, G. A. Snyder, L. A. Taylor, Science 278, 1098 (1997).
6. J. H. Jones, H. Palme, in Origin of the Earth and Moon, R. M. Canup, K. Righter, Eds. (Univ. Arizona Press, Tucson, AZ, 2000), pp. 197–216.
7. C. K. Shearer, H. E. Newsom, Geochim. Cosmochim. Acta 64, 3599 (2000).
8. I. Leya, R. Wieler, A. N. Halliday, Earth Planet. Sci. Lett. 175, 1 (2000).
9. D. C. Lee, A. N. Halliday, I. Leya, R. Wieler, U. Wiechert, Earth Planet. Sci. Lett. 198, 267 (2002).
10. H. Wänke et al., Proc. Sec. Lunar Planet. Sci. Conf. 2, 1187 (1971).
11. C. K. Shearer, J. J. Papike, Am. Mineral. 84, 1469 (1999).
12. P. H. Warren, J. T. Wasson, Rev. Geophys. Space Phys. 17, 73 (1979).
13. H. Palme, H. Wänke, Proc. Lunar Sci. Conf. 6, 1179 (1975).
14. K. Righter, C. K. Shearer, Geochim. Cosmochim. Acta 67, 2497 (2003).
15. I. Leya, R. Wieler, A. N. Halliday, Geochim. Cosmochim. Acta 67, 529 (2003).
16. L. E. Nyquist et al., Geochim. Cosmochim. Acta 59, 2817 (1995).
17. H. Palme, W. Rammensee, Lunar Planet. Sci. XII, 796 (1981).
18. T. Kleine, C. Münker, K. Mezger, H. Palme, Nature 418, 952 (2002).
19. Q. Z. Yin et al., Nature 418, 949 (2002).
20. S. B. Jacobsen, Annu. Rev. Earth Planet. Sci. Lett. 33, 531 (2005).
21. A. N. Halliday, Nature 427, 505 (2004).
22. T. Kleine, K. Mezger, H. Palme, E. Scherer, C. Münker, Earth Planet. Sci. Lett. 228, 109 (2004).
23. L. T. Elkins-Tanton, J. A. Van Orman, B. H. Hager, T. L. Grove, Earth Planet. Sci. Lett. 196, 239 (2002).
24. S. C. Solomon, J. Longhi, Proc. Lunar Sci. Conf. 8, 583 (1977).
25. H. Palme, Geochim. Cosmochim. Acta 41, 1791 (1977).
26. R. W. Carlson, G. W. Lugmair, Earth Planet. Sci. Lett. 45, 123 (1979).
27. T. Kleine, K. Mezger, H. Palme, E. Scherer, C. Münker, Geochim. Cosmochim. Acta, in press.
28. T. Kleine, K. Mezger, C. Münker, H. Palme, A. Bischoff, Geochim. Cosmochim. Acta 68, 2935 (2004).
29. T. Kleine, K. Mezger, H. Palme, E. Scherer, C. Münker, Earth Planet. Sci. Lett. 231, 41 (2005).
30. We thank NASA for providing the samples for this study and I. Leya, R. Wieler, L. Borg, T. Grove, T. Irving, S. Jacobsen, L. Nyquist, and two anonymous reviewers for their comments. E. Scherer supported the MC-ICPMS in Münster, and C. Münker provided aliquots of the whole-rock samples. This study was supported by the Deutsche Forschungsgemeinschaft as part of the research priority program "Mars and the terrestrial planets" and by a European Union Marie Curie postdoctoral fellowship to T.K.

The Importance of Land-Cover Change in Simulating Future Climates

Johannes J. Feddema,[1]* Keith W. Oleson,[2] Gordon B. Bonan,[2] Linda O. Mearns,[2] Lawrence E. Buja,[2] Gerald A. Meehl,[2] Warren M. Washington[2]

Adding the effects of changes in land cover to the A2 and B1 transient climate simulations described in the Special Report on Emissions Scenarios (SRES) by the Intergovernmental Panel on Climate Change leads to significantly different regional climates in 2100 as compared with climates resulting from atmospheric SRES forcings alone. Agricultural expansion in the A2 scenario results in significant additional warming over the Amazon and cooling of the upper air column and nearby oceans. These and other influences on the Hadley and monsoon circulations affect extratropical climates. Agricultural expansion in the mid-latitudes produces cooling and decreases in the mean daily temperature range over many areas. The A2 scenario results in more significant change, often of opposite sign, than does the B1 scenario.

As anthropogenic impacts on Earth's surface continue to accelerate, the effects of these actions on future climate are still far from known (1–3). Historical land-cover conversion by humans may have decreased temperatures by 1° to 2°C in mid-latitude agricultural regions (4–9). Simulations of tropical deforestation (10–12) and potential future human land-cover impacts project a warming of 1° to 2°C in deforested areas (13, 14), with possible ex-

tratropical impacts due to teleconnection processes (7, 11, 13, 15). However, most of these experiments have been performed in uncoupled or intermediate-complexity climate models and have not followed the proposed framework of the Intergovernmental Panel on Climate Change (IPCC) Special Report on Emissions Scenarios (SRES) (16). The study described here evaluated whether future land use decisions, based on assumptions similar to those used to create the IPCC SRES atmospheric forcing scenarios, could alter the outcomes of two future IPCC SRES climate simulations.

Land-cover impacts on global climate can be divided into two major categories: biogeochemical and biogeophysical (2, 14–18).

Biogeochemical processes affect climate by altering the rate of biogeochemical cycles, thereby changing the chemical composition of the atmosphere. To some extent, these emissions are included in the IPCC climate change assessments (1). Biogeophysical processes directly affect the physical parameters that determine the absorption and disposition of energy at Earth's surface. Albedo, or the reflective properties of Earth's surface, alters the absorption rate of solar radiation and hence energy availability at Earth's surface (4–19). Surface hydrology and vegetation transpiration characteristics affect how energy received by the surface is partitioned into latent and sensible heat fluxes (4–19). Vegetation structure affects surface roughness, thereby altering momentum and heat transport (12). Summarizing the effects of land-cover change on climate has been difficult because different biogeophysical effects offset each other in terms of climate impacts (16), and, on global and annual scales, regional impacts are often of opposite sign and are therefore not well represented in annual global average statistics (7, 16).

For this study, we used the fully coupled Department of Energy Parallel Climate Model (DOE-PCM) (20, 21) to simulate combined land-cover and atmospheric forcings for the A2 and B1 IPCC SRES scenarios (22). Atmospheric forcings were identical to those used in previous IPCC SRES scenario experiments, resulting in a 1°C warming for the low-impact B1 scenario and a 2°C warming for the high-impact A2 scenario (20). To simulate future land-cover change, we used the Integrated Model to Assess the Global Environment (IMAGE) 2.2 IPCC SRES land-cover projections (7, 22–24) and DOE-PCM natural vegetation data to create land-cover data sets

[1]Department of Geography, University of Kansas, Lawrence, KS 66045, USA. [2]National Center for Atmospheric Research, Post Office Box 3000, Boulder, CO 80307, USA.

*To whom correspondence should be addressed. E-mail: feddema@ku.edu